

# Engineering Notes

# Atmospheric Density Uncertainty Quantification for Satellite Conjunction Assessment

David J. Gondelach\*

Vyoma, GmbH, 64295 Darmstadt, Germany
and

Richard Linares<sup>†</sup> and Peng Mun Siew<sup>‡</sup>

Massachusetts Institute of Technology, Cambridge,

Massachusetts 02139

https://doi.org/10.2514/1.G006481

#### Nomenclature

$\boldsymbol{A}$	=	state matrix of the reduced-order system
$A_p$	=	geomagnetic $A_p$ index, 2 nano Tesla (2nT)
a	=	semimajor axis, km
В	=	input matrix of the reduced-order system
$c_i$	=	time-dependent coefficient for spatial mode i
$F_{10.7}$	=	solar radio flux with wavelength of 10.7 cm, solar
		flux unit (sfu)
$\boldsymbol{G}$	=	Jacobian matrix
P	=	covariance
$P_c$	=	probability of collision
p, f, g, h,	=	modified equinoctial elements ( $p$ is the semilatus
k, L		rectum, km; L is the true longitude, rad)
$R_i$	=	body radius of <i>i</i> th object, km
r	=	position vector, km
$oldsymbol{U}$	=	left-singular vectors
u	=	input to the reduced-order system
V	=	right-singular vectors
$\boldsymbol{v}$	=	velocity vector, km/s
x	=	neutral mass density in the log scale, kg/m <sup>3</sup>
$\boldsymbol{z}$	=	reduced-order state
$egin{array}{c} eta \ \Delta_g \ \delta \end{array}$	=	ballistic coefficient, kg/m <sup>2</sup>
$\Delta_g$	=	global model parameter errors
δ	=	errors in the initial state
$\mu$	=	mean
ρ	=	neutral mass density, kg/m <sup>3</sup>
$oldsymbol{\Sigma}$	=	singular values
$\sigma$	=	standard deviation
$\sigma^*$	=	multiplicative standard deviation
$\Phi_i$	=	spatial mode i

Subscripts

c = continuous system k = data at time step k

Received 30 September 2021; revision received 22 April 2022; accepted for publication 23 April 2022; published online 23 May 2022. Copyright © 2022 by the American Institute of Aeronautics and Astronautics, Inc. All rights reserved. All requests for copying and permission to reprint should be submitted to CCC at www.copyright.com; employ the eISSN 1533-3884 to initiate your request. See also AIAA Rights and Permissions www.aiaa.org/randp.

n = nth space object x = x component y = y component z = z component

#### Superscripts

w/o = without density error  $\rho$  = with density error

 $\rho$ , corr = with density error and cross-correlation correction

#### I. Introduction

 ${f T}$  HE growing population of satellites and orbital debris in Earth's orbit increases the spatial density, and therefore the risk of collision events between objects. Therefore, satellites and other objects need to be tracked and their orbits predicted to detect close encounters and assess the risk of collision. Accurate calculation of the probability of collision  $P_c$  requires both accurate prediction of the orbit and accurate estimation of the uncertainty in the orbit prediction. The main sources of error in orbit prediction are errors in observational data, limited knowledge of object properties (shape, mass, and material) and attitude, and errors in the modeling of the atmosphere needed for drag calculations [1].

Uncertainties in the initial state due to measurement errors can be estimated during orbit determination. In addition, uncertainties in the drag coefficient, frontal area, and mass can be combined in the ballistic coefficient  $\beta$ , which can be solved for in orbit determination and can be included in the covariance. On the other hand, errors in the atmospheric density estimates are often unknown or not well characterized. Vallado and Finkleman [2] reported an average one sigma accuracy of 10 to 15% for empirical density models. However, the error in density depends on the employed density model as well as on the space weather conditions and location [3]. Therefore, there is a strong need to both accurately estimate density and the uncertainty in the density. The goal of this work is to quantify the uncertainty in atmospheric density and take these uncertainties into account for collision probability calculations.

The current state of practice by the U.S. Space Force for incorporating uncertainty in the atmospheric density is by adding the uncertainty in the density to the ballistic coefficient variance. A drawback of this approach is that the density uncertainty scale is equal in all atmospheric regions; whereas in reality, the density error is not uniform over the density field. This aspect becomes important when the conjunction between two significantly different orbits (e.g., different mean altitude or different orbital plane) is considered.

Several studies have looked into the effect of uncertainty on the atmospheric density in orbit prediction [4–6]; however, few have considered their effect on the probability of collision. In addition, most of these studies focused on the error in atmospheric density due to inaccurate space weather inputs and forecasts because these errors become dominant for orbit prediction of several days. However, for orbit determination and short-term orbit predictions, the error in the density model itself is expected to be larger. Therefore, density models need to be calibrated and the uncertainties in the model must be estimated. Several techniques exist for density model calibration [7–9]. However, these techniques do not provide direct estimates of the uncertainty in the density. In addition, the calibration is carried out using static atmospheric models; therefore, it is not possible to predict how uncertainties in the density evolve over time (only the statistics of historical predictions can be studied). There is, therefore, a strong

<sup>\*</sup>Astrodynamics Specialist, Berliner Allee 65; david.gondelach@vyoma.

<sup>&</sup>lt;sup>†</sup>Boeing Assistant Professor, Department of Aeronautics and Astronautics, 77 Massachusetts Avenue; linaresr@mit.edu. Senior Member AIAA.

<sup>&</sup>lt;sup>‡</sup>Postdoctoral Associate, Department of Aeronautics and Astronautics, 77 Massachusetts Avenue; siewpm@mit.edu.

need for the quantification of uncertainty in density models and the propagation of these uncertainties into the future.

Two studies that considered the effect of density errors on the collision probability were carried out by Bussy-Virat et al. [10] and Hejduk and Snow [11]. Bussy-Virat et al. [10] analyzed the effect of errors in the future space weather prediction on the  $P_c$  and used different future space weather scenarios to obtain a probability density function (PDF) for the  $P_c$ . For this, they considered errors in the solar activity proxies  $F_{10.7}$  and  $A_p$  but did not consider errors in the density model itself. Hejduk and Snow [11] studied how the severity level of conjunctions changes due to errors in density and density uncertainties. They assumed density errors of a factor of 0.5 to 2.0 with respect to the model density due to model and space weather forecast errors, and they used a consider parameter to include density uncertainties in the covariance. They analyzed the effect of the error and uncertainties on the  $P_c$ , and showed that ignoring density uncertainties can lead to failure to detect severe conjunction events. Hejduk and Snow did not, however, consider the cross correlation in position uncertainties due to density errors.

If an estimate of the uncertainty in density is available, one can study the effect of density errors on the probability of collision. The most widely used technique, called linear or two-dimensional  $P_c$  estimation, uses the covariances of the two objects at the time of closest approach (TCA) to compute the  $P_c$ . It is important to account for correlation in the position errors when computing the joint position covariance for probability of collision calculation [12,13]. When two objects fly through the same atmosphere, the position errors due to errors in the density will be correlated, and thus one should account for the cross correlation [12,13]; however, most previous work does not consider this effect on the  $P_c$  calculation.

In this Note, we propose a new technique to estimate and include the uncertainty in atmospheric density for conjunction assessment. For this, we use a recently developed dynamic density model that enables density forecasting [14]. Common physics-based models of the thermosphere, such as Global Ionosphere Thermosphere Model (GITM) and Thermosphere Ionosphere Electrodynamics General Circulation Model (TIE-GCM), require solving Navier-Stokes equations over a high-dimensional discretized spatial grid involving 10<sup>4</sup>10<sup>6</sup> state variables, which is computationally expensive. On the other hand, empirical models are able to produce fast prediction but have a limited forecasting capability. Traditionally, correction to empirical density models is achieved by estimating scale parameter(s) that correct the models to match the measured orbital data [15,16]. Mehta et al. [14] used reducedorder modeling to develop a low-dimensional dynamic model for the thermospheric density. This model enables efficient estimation of the density using a Kalman filter. Improvement in the accuracy of the estimated density was demonstrated by assimilating accelerometerderived density measurements [17], two-line element (TLE) data [18], satellite position measurements [17], and radar and Global Positioning System tracking data [20]. The authors showed that density estimates based on TLE data were more accurate than the Jacchia-Bowman 2008 (JB2008)§ and 2001 United States Naval Research Laboratory Mass Spectrometer and Incoherent Scatter Radar Exosphere (NRLMSISE-00) models [18]. In addition, the estimates for the uncertainty in estimated density were obtained. These density uncertainties depend on the latitude, local solar time, and altitude. In addition, the uncertainty was found to be dependent on the epoch (i.e., solar activity) and measurement data. This is a significant improvement over a single global density error estimate that does not include the location and time dependency of density errors. Moreover, the density prediction depends on the solar activity such that the predicted density uncertainty also depends on the future space weather.

We use the dynamic model to estimate both the global atmospheric density using TLE data and the uncertainty in the estimated density. The dynamic model is then used to predict the future density and corresponding uncertainty. By propagating the orbit and the

atmospheric state simultaneously, and by employing uncertainty propagation, we can obtain the uncertainty in the orbit due to uncertainty in both the initial orbital state and in the density model. Finally, we use the orbit and covariance computed for two space objects to calculate the probability of collision between the objects and compare the result with  $P_c$  in cases where density uncertainties are not considered. Here, the effect of cross correlation due to density errors is considered as well.

In previous work, Gondelach and Linares demonstrated the use of the dynamic density model for accurate density estimation and density uncertainty quantification [18]. The contributions of this work are as follows:

- 1) The future density uncertainty is computed by propagating the uncertainty during the density prediction.
- 2) The orbital state uncertainty that includes uncertainty due to the density errors is computed by propagating the state and density uncertainties simultaneously.
- 3) The probability of collision is computed using position covariances that include uncertainty due to density.
- 4) The combined position covariance used for collision probability calculation is adjusted to account for the effect of cross correlation in the position uncertainties due to density errors.
- 5) The effect of density uncertainties and the effect of cross correlation on the probability of collision estimate are assessed.
- 6) The estimated collision probability is compared with collision probabilities computing using Monte Carlo analysis.

In the following, first, the methods employed for the new approach are discussed. After that, the test cases for conjunction assessment are presented.  $P_c$  is computed for the different scenarios, with and without considering density uncertainties and cross-correlation effects. Finally, the results are discussed and conclusions are drawn.

#### II. Methodology

First, we briefly introduce the development of the dynamic reduced-order density model (RODM). After that, density estimation using the dynamic model and TLE data with a Kalman filter is discussed. Finally, the technique of computing the collision probability is presented.

#### A. Dynamic Reduced-Order Density Model

The goal of the development of a RODM is to enable computationally efficient forecasting of atmospheric density. This is achieved by reducing the dimension of atmospheric state with respect to physics-based models and by deriving a dynamic model for the reduced-order state. The main idea of reduced-order modeling is to reduce the dimensionality of the state space while retaining maximum information. In our case, the full state space consists of the neutral mass density values on a dense uniform grid in latitude, local solar time, and altitude. First, to make the problem tractable, the statespace dimension is reduced using proper orthogonal decomposition (POD). Second, a linear dynamic model is derived by applying dynamic mode decomposition with control (DMDC). Under the DMDC formulation, the reduced-order states are approximated as a linear process, where the current reduced-order state only depends on the reduced-order state, linear and nonlinear space weather\*\* indices from the previous epoch. Details for the POD and DMDC formulation can be found in Ref. [18].

In this work, we use a RODM based on density data from the JB2008 density model. We computed hourly density data on a dense grid in latitude, local solar time, and altitude over 12 years from 1999 to 2010. The data were then used to perform POD and DMDC to obtain our dynamic RODM for the thermosphere.

<sup>§</sup>Model available online at http://sol.spacenvironment.net/jb2008/code.html [retrieved 10 May 2022].

Model available online at https://www.brodo.de/space/nrlmsise [retrieved 10 May 2022].

<sup>\*\*</sup>Data available online at http://celestrak.com/SpaceData/ [retrieved 10 May 2022] and http://sol.spacenvironment.net/jb2008/indices.html [retrieved 10 May 2022].

#### **B.** Density Estimation

We can estimate the reduced-order density state using the RODM. In this work, this is achieved by simultaneously estimating the reduced-order density state and the orbital states of objects by data assimilation of TLE data, as described in a previous paper by Gondelach and Linares [18]. A square-root unscented Kalman Filter is used as the estimation filter [21]. The state x that is estimated consists of the osculating orbital states [expressed in modified equinoctial elements (MEEs)], the ballistic coefficient of the objects  $\beta_i$ , and the reduced-order density state z:

$$\mathbf{x} = \begin{bmatrix} p_1, f_1, g_1, h_1, k_1, L_1, \beta_1, & \dots & p_n, f_n, g_n, h_n, k_n, L_n, \beta_n, & \mathbf{z}^T \end{bmatrix}^T$$
(1)

where n is the number of objects. The measurements consist of osculating orbital states extracted from TLE data (expressed in MEEs). The reduced-order density state z is propagated using the RODM. The orbits are propagated in the J2000 Earth-centered inertial reference frame by considering geopotential acceleration (Earth Gravitational Model 2008 (EGM2008) with  $20 \times 20$  harmonics) and atmospheric drag computed using the RODM. By using a subset of well-tracked objects (with accurately estimated  $\beta$ ) that are evenly distributed in the atmosphere, we are able to accurately estimate the global thermospheric density. For more details about the orbital dynamical model and process as well as the measurement noise used for estimation, we refer the reader to Ref. [18].

#### C. Uncertainty Estimation

From the Kalman filter estimation, we obtain both an estimate for the state x and an estimate of the covariance  $P_x$ :

$$P_{x} = \begin{bmatrix} \sigma_{p_{1}}^{2} & \sigma_{p_{1}f_{1}} & \sigma_{p_{1}g_{1}} & \dots & \dots & \dots & \dots \\ \sigma_{p_{1}f_{1}} & \sigma_{f_{1}}^{2} & \sigma_{f_{1}g_{1}} & \dots & \dots & \dots & \dots \\ \sigma_{p_{1}g_{1}} & \sigma_{f_{1}g_{1}} & \sigma_{g_{1}}^{2} & \dots & \dots & \dots & \dots \\ \vdots & \vdots & \vdots & \ddots & \dots & \dots & \dots \\ \vdots & \vdots & \vdots & \vdots & \vdots & \sigma_{z_{1}}^{2} & \dots & \sigma_{z_{1}z_{r}} \\ \vdots & \vdots & \vdots & \vdots & \vdots & \ddots & \vdots \\ \vdots & \vdots & \vdots & \vdots & \vdots & \sigma_{z_{1}z_{r}} & \dots & \sigma_{z_{r}z_{r}}^{2} \end{bmatrix}$$

The lower right part of  $P_x$  contains the covariance of the reducedorder density state  $z(P_z)$ . This covariance can be used to compute the effect of density uncertainty on the position uncertainty, and thus on the collision probability. In addition,  $P_z$  can be converted to uncertainty in the physical density. Using a single row of the projection matrix  $U_r$  that corresponds to one grid point i in the full space  $U_{r,i}$ , we obtain the uncertainty in the density as follows:

$$\sigma_{\tilde{i}_i}^2 = \boldsymbol{U}_{r,i} \boldsymbol{P}_z \boldsymbol{U}_{r,i}^T \tag{2}$$

where  $\sigma_{\tilde{x}i}^2$  is the variance of the variation of density  $\tilde{x}$  in log space at grid point i, see Ref. [18].

# D. Collision Probability Calculation

We use Alfano's method [22] to calculate the probability of collision  $P_c$ . This technique provides an accurate estimate of the true  $P_c$  if the PDF of the position is Gaussian and the duration of the encounter between the two objects is very short such that the PDF is constant during the encounter. In this work, we have assessed the Gaussianity and short encounter duration for our test cases. In addition, we will assume that the distance of close approach (DCA) is not affected by the error in the density; whereas in reality, it is.

However, if the change in DCA due to uncertainties is small compared to the covariance size, then the effect on  $P_c$  is small.

In Alfano's method [22],  $P_c$  is computed by projecting the combined position covariance and relative miss distance on the encounter plane, and computing the probability that the miss distance is smaller than the combined body radius.  $P_c$  can be computed using [23]

$$P_{c} = \frac{1}{\sqrt{8\pi\sigma_{x}}} \int_{0}^{R} \left[ \operatorname{erf}\left(\frac{y_{m} + \sqrt{R^{2} - x^{2}}}{\sqrt{2}\sigma_{y}}\right) + \left(\frac{-y_{m} + \sqrt{R^{2} - x^{2}}}{\sqrt{2}\sigma_{y}}\right) \right] \times \left[ \exp\left(\frac{-(x + x_{m})^{2}}{2\sigma_{x}^{2}}\right) + \exp\left(\frac{-(-x + x_{m})^{2}}{2\sigma_{x}^{2}}\right) \right] dx$$
(3)

where

$$\operatorname{erf}(z) = \frac{2}{\sqrt{\pi}} \int_0^z e^{-t^2} dt \tag{4}$$

is the error function, and  $R=R_1+R_2$  is the combined body radius of the two objects. For this integral, the x axis is aligned with the major axis of the projected covariance such that the projected covariance is given by the standard deviations  $\sigma_x$  and  $\sigma_y$  and the relative position is given by  $x_m$  and  $y_m$ . More information on Alfano's method can be found in Refs. [22,23]. In Sec. II.F, we will show how to compute the combined covariance  $P_m$  that accounts for cross correlation between the object's position uncertainties due to density errors.

# E. Uncertainty Propagation

To compute  $P_c$ , we need to calculate position covariances  $P_1$  and  $P_2$  of the two objects at the TCA. For this, we augment position covariance matrix  $P_i$  of the object with the covariance of the object's ballistic coefficient and the covariance of the reduced-order state; then, we propagate this joint covariance using an unscented transformation (i.e., sigma point propagation) [21,24]. For uncertainty propagation, the orbital state is expressed in modified equinoctial elements to mitigate the departure from "Gaussianity" of the state PDF under the nonlinear propagation with respect to Cartesian coordinates. After computing the covariance in MEEs at the TCA, the covariance is converted to Cartesian space using unscented transformation to obtain the position covariance needed in Alfano's method [22]. Note that if the position PDF becomes strongly non-Gaussian, then Alfano's method does not provide an accurate approximation of  $P_c$  anymore. For the scenarios that we are interested in, the objects are assumed to be well tracked such that the position PDF does not become strongly non-Gaussian throughout the conjunction scenario. The Gaussian assumption for the position PDF during the conjunction scenario is analyzed in Sec. IV.B.

#### F. Cross Correlation

Casali et al. [13] described a technique to consider the effect of cross correlation of orbital errors on the probability of collision. In this section, we follow the derivation by Casali et al. [13] to obtain an equation to correct for cross correlation due to density errors in the calculation of  $P_c$ . Starting from the definition of the miss distance  $\mathbf{r}_m = \mathbf{r}_2 - \mathbf{r}_1$ , the mean and covariance of the miss distance are given by

$$\mu_m = E[\mathbf{r}_m] = E[\mathbf{r}_2 - \mathbf{r}_1] = E[\mathbf{r}_2] - E[\mathbf{r}_1] = \mu_2 - \mu_1$$
 (5)

$$P_m = P_2 + P_1 - E[(r_2 - \mu_2)(r_1 - \mu_1)^T] - E[(r_1 - \mu_1)(r_2 - \mu_2)^T]$$
(6)

When the position errors in  $r_1$  and  $r_2$  are independent, the cross-correlation terms are zero such that  $P_m = P_2 + P_1$ . This is generally the assumption when performing conjunction assessment using linear techniques because errors from orbit determination are assumed to be statistically independent.

Now, let us assume that the errors in the orbit predictions are due to both errors in the initial state  $\delta$  and global model parameter errors  $\Delta_g$ . Then, for the position deviations at the TCA, we can write

$$\mathbf{r}_i - \boldsymbol{\mu}_i = \boldsymbol{\Phi}_i \boldsymbol{\delta}_i + \boldsymbol{G}_i \boldsymbol{\Delta}_g \tag{7}$$

where  $\Phi$  is the state transition matrix that maps the deviation in the initial state  $\delta$  to a deviation in the state at the TCA, and G is a state transition matrix that provides the linear approximation of the effect of the error  $\Delta_g$  on the state at the TCA over the prediction window as  $\Phi$  does. Using these expressions for the state deviations, we obtain from Eq. (6)

$$P_{m} = E[(\mathbf{\Phi}_{2}\boldsymbol{\delta}_{2} + G_{2}\boldsymbol{\Delta}_{g})(\mathbf{\Phi}_{2}\boldsymbol{\delta}_{2} + G_{2}\boldsymbol{\Delta}_{g})^{T}]$$

$$+ E[(\mathbf{\Phi}_{1}\boldsymbol{\delta}_{1} + G_{1}\boldsymbol{\Delta}_{g})(\mathbf{\Phi}_{1}\boldsymbol{\delta}_{1} + G_{1}\boldsymbol{\Delta}_{g})^{T}]$$

$$- E[(\mathbf{\Theta}_{2}\boldsymbol{\delta}_{2} + G_{2}\boldsymbol{\Delta}_{g})(\mathbf{\Theta}_{1}\boldsymbol{\delta}_{1} + G_{1}\boldsymbol{\Delta}_{g})^{T}]$$

$$- E[(\mathbf{\Theta}_{1}\boldsymbol{\delta}_{1} + G_{1}\boldsymbol{\Delta}_{e})(\mathbf{\Theta}_{2}\boldsymbol{\delta}_{2} + G_{2}\boldsymbol{\Delta}_{e})^{T}]$$

$$(8)$$

Now, we assume there is no dependence between the errors due to orbit determination and between the error due to orbit determination and the global error (i.e.,  $E[\boldsymbol{\delta}_1\boldsymbol{\delta}_2^T]=0$  and  $E[\boldsymbol{\delta}_1\boldsymbol{\Delta}_g^T]=E[\boldsymbol{\delta}_2\boldsymbol{\Delta}_g^T]=0$ ), whereas  $E[\boldsymbol{\Delta}_g\boldsymbol{\Delta}_g^T]=\boldsymbol{P}_g$ . We then get

$$\mathbf{P}_{m} = \mathbf{\Phi}_{2} \mathbf{P}_{2,0} \mathbf{\Phi}_{2}^{T} + \mathbf{\Phi}_{1} \mathbf{P}_{1,0} \mathbf{\Phi}_{1}^{T} + (\mathbf{G}_{2} \mathbf{P}_{g} \mathbf{G}_{2}^{T} + \mathbf{G}_{1} \mathbf{P}_{g} \mathbf{G}_{1}^{T} 
- \mathbf{G}_{2} \mathbf{P}_{g} \mathbf{G}_{1}^{T} - \mathbf{G}_{1} \mathbf{P}_{g} \mathbf{G}_{2}^{T}) 
= (\mathbf{\Phi}_{2} \mathbf{P}_{2,0} \mathbf{\Phi}_{2}^{T} + \mathbf{G}_{2} \mathbf{P}_{g} \mathbf{G}_{2}^{T}) + (\mathbf{\Phi}_{1} \mathbf{P}_{1,0} \mathbf{\Phi}_{1}^{T} + \mathbf{G}_{1} \mathbf{P}_{g} \mathbf{G}_{1}^{T}) 
- \mathbf{G}_{2} \mathbf{P}_{g} \mathbf{G}_{1}^{T} - \mathbf{G}_{1} \mathbf{P}_{g} \mathbf{G}_{2}^{T} 
= \mathbf{P}_{2} + \mathbf{P}_{1} - \mathbf{G}_{2} \mathbf{P}_{e} \mathbf{G}_{1}^{T} - \mathbf{G}_{1} \mathbf{P}_{e} \mathbf{G}_{2}^{T}$$
(9)

where  $P_{2,0}$  and  $P_{1,0}$  are the initial covariances representing errors in  $\delta$ . In our case, the global errors  $\Delta_g$  are given by the covariance of the reduced-order density state  $P_z$ . Therefore, to calculate the cross correlation in the state errors due  $\Delta_g$ , we need to compute matrices  $G_1$  and  $G_2$  that give the first-order relation between errors in the density and errors in the states at the TCA.

Matrix G is a Jacobian that contains the partial derivatives of the position r at the TCA with respect to the reduced-order density state at the initial epoch  $z_0$ :

$$G = \frac{\partial \mathbf{r}}{\partial z_0} = \begin{bmatrix} \frac{\partial r_x}{\partial z_{0,1}} & \cdots & \frac{\partial r_x}{\partial z_{0,r}} \\ \vdots & \ddots & \vdots \\ \frac{\partial r_z}{\partial z_{0,1}} & \cdots & \frac{\partial r_z}{\partial z_{0,r}} \end{bmatrix}$$
(10)

These partial derivatives are approximated using central finite differences. For this, we use the sigma points that we have already computed for propagating the covariance such that the partials are approximated as, e.g.,

$$\frac{\partial r_x}{\partial z_{0,1}} \approx \frac{r_x(\Delta z_{0,1}) - r_x(-\Delta z_{0,1})}{2\Delta z_{0,1}} \tag{11}$$

where  $r_x(\Delta z_{0,1})$  is the value of  $r_x$  when a change of  $\Delta z_{0,1}$  is applied to the initial state. These values are taken from the results of the sigma point propagation. Note that we did not notice any numerical instability in approximating the partial derivatives using sigma points; however, we would like to caution the readers on the possibility of numerical instability; alternatively, the readers can opt to use higher-order stencil approaches for better accuracy and numerical stability. Once  $G_1$  and  $G_2$  are computed, we can calculate the covariance of the miss distance  $P_m$  that accounts for cross correlation due to atmospheric density errors using Eq. (9). This  $P_m$  is then used in Alfano's

method [22] to calculate the  $P_{\it c}$  that accounts for the effect of cross correlation.

# III. Test Cases

To test our new approach for computing the effect of density uncertainties on  $P_c$ , we generated artificial conjunction scenarios. The test case consists of two nearly identical near-polar orbits at about 400 km altitude that have a different right ascension of the ascending node such that they have a conjunction point at high latitude; see Table 1. The conjunction was set to take place on 13 February 2003, at 00:00:00 hrs Coordinated Universal Time (UTC). The conjunction assessment is carried out over a two-day window such that the start epoch for orbit prediction for  $P_c$  estimation was two days earlier on 11 February 2003, at 00:00:00 hrs UTC. The initial conditions of the orbits two days before conjunction were obtained by starting from the conjunction point and propagating the orbits backward in time to the start epoch (i.e., two days before the time of conjunction) using the nominal atmospheric density. Six different conjunction scenarios were created by varying the  $\beta$  of one of the objects and by changing the DCA via changing the in-track position of one of the objects at the TCA; see Table 2. The combined hard-body radius R was set to 2 m.

To obtain accurate density and covariance estimates, we estimated the reduced-order density state and its covariance over a 10-day window before the conjunction scenario from 1 February to 11 February 2003. The reduced-order density state on 1 February was initialized using the JB2008 modeled density field on that day [18]. During the 10-day estimation, TLE data from 17 objects (with North America Aerospace Defense Command (NORAD) catalog identification numbers 63, 165, 614, 2153, 2622, 4221, 6073, 7337, 8744, 12,138, 12,388, 14,483, 20,774, 23,278, 26,405, 27,391, and 27,392) were assimilated into the reduced-order density state to obtain an accurate initial reduced-order density state and its covariance for the two-day conjunction scenario. The reduced-order density state was then propagated forward for two days to obtain a prediction of the atmospheric density, which is the nominal density for the conjunction assessment

For the conjunction assessment, we assume uncertainties in the initial state, ballistic coefficient, and reduced-order density. The assumed uncertainty in the initial states expressed in MEEs is shown in Table 3. These uncertainties were obtained from the orbit determination for the Gravity Recovery and Climate Experiment (GRACE) - A satellite using TLE data, and subsequently arbitrary scaled by a factor of 0.1 (i.e., reduced by one order of magnitude) to obtain magnitudes for the uncertainty that were more realistic when having access to accurate orbital data.  $\beta$  is assumed to have a 1- $\sigma$  error of 0.5%:  $\sigma_{\beta} = 0.005 \cdot \beta$ .

 $P_c$  is computed using Alfano's method [22] with and without considering density uncertainties and with and without considering cross correlation when computing the combined position covariance. Finally, to estimate the true  $P_c$  with density uncertainty, we perform

Table 1 Nominal orbits at collision point

Orbit	a, km	e	i, deg	Ω, deg	$\omega$ , deg	$\nu$ , deg
1	6778.13630	0.00300	89.0	0.0	90.0	0.41418532
2	6778.13630	0.00300	89.0	45.0	90.0	-0.41418532

Table 2 Six conjunction scenarios with different DCAs and object ballistic coefficients  $\beta$ 

Scenario	Test case identification	DCA, km	$\beta_1$ , m <sup>2</sup> /kg	$\beta_2$ , m <sup>2</sup> /kg
Same $\beta$	S0	0.00031	0.01	0.01
	S1	0.92375	0.01	0.01
	S2	1.84756	0.01	0.01
Different $\beta$	D0	0.00015	0.01	0.001
	D1	0.92412	0.01	0.001
	D2	1.84756	0.01	0.001

Table 3 Assumed 1- $\sigma$  uncertainty in the initial MEE states

State	Uncertainty
$\sigma_p$	$1.40546843775429 \times 10^{-4} \text{ km}$
$\sigma_f$	$1.54877138747695 \times 10^{-7}$
$\sigma_g$	$1.54788273902825 \times 10^{-7}$
$\sigma_h$	$2.50908224756075 \times 10^{-7}$
$\sigma_k$	$1.36880945273941 \times 10^{-7}$
$\sigma_L$	$2.28039102756189 \times 10^{-7}$ rad

Monte Carlo analyses by sampling initial densities from the density PDF and calculating the resulting  $P_c$  by considering only initial state uncertainty. From the Monte Carlo analyses, we obtain a mean  $P_c$ , which is the expected  $P_c$  value.

#### IV. Results

#### A. Density Estimation and Uncertainty Quantification

The accuracy of the RODM-estimated densities based on TLE data in 2003 and 2007 was presented in previous work by Gondelach and Linares [18]. Here, we will have a closer look at the corresponding estimated uncertainties. Figure 1 shows the error and estimated  $3-\sigma$  error in orbit-averaged density with respect to Challenging Minisatellite Payload (CHAMP) accelerometer-derived densities over the year 2007. (The estimated  $3-\sigma$  error jumps up every 15 days because the density estimation was restarted every 15 days to enable parallel calculation. After a couple of days of estimation, the estimated density becomes more accurate and estimated uncertainty drops.) Note that 97.0% of the errors are within the estimated  $3-\sigma$  error bounds. This shows that estimated uncertainty provides a good estimate of the true error in density. (The CHAMP and GRACE densities used in this work were derived by Sutton [26]).

The atmospheric density field and its associated uncertainties 10 days before our test case (1 February 2013) were propagated forward and assimilated with TLE data to 11 February 2003. The uncertainty in the estimated density on 11 February 2003, at 400 and 500 km altitudes is shown in Fig. 2a. The plots show the multiplicative standard deviation of  $\sigma^* = 10^\sigma$ , where  $\sigma$  is the standard deviation in log space computed using Eq. (2). This serves as an initial condition of the atmospheric density reduced-order state for our start epoch. For the conjunction assessment, the density and uncertainty were propagated for two days up to the TCA. In this two-day window, the solar activity was moderately high; the  $F_{10.7}$  was about 135, and the  $A_p$  varied between 5 and 27. Figure 2b shows the uncertainty after the two-day prediction. One can see that the uncertainties have grown as a result of the atmospheric dynamics and external forcing by solar activity.

To demonstrate the accuracy of the density and uncertainty prediction over our conjunction epoch, we compared the predicted density and uncertainty along CHAMP's orbit with CHAMP accelerometer-derived densities. Figure 3 shows the two-day predicted density along CHAMP's orbit (at about a 415 km altitude) together with NRLMSISE-00, JB2008, and accelerometer-derived densities. The densities predicted using the RODM are accurate, with a maximum orbit-averaged density error of 12%; see Fig. 3d. On the other hand, Figs. 3a and 3c show that the density according to the NRLMSISE-00 model is significantly biased in this time window. The RODM-estimated density and 3- $\sigma$  uncertainty are shown in Fig. 3b. In the two-day window, 56% of the accelerometer-derived densities are within the 3- $\sigma$  bounds. This means that the true error in local density is larger than estimated. The uncertainty in the local density is probably underestimated because the short-term fluctuations in density cannot be detected from TLE data, which are generated from multiday observation data.

#### B. Gaussianity

For accurate estimation of the  $P_c$  using Alfano's method [22], the position covariance needs to be Gaussian. We performed a Monte Carlo analysis to assess the Gaussianity of one of the position PDFs in test case S0. For this, we sampled 1000 initial conditions from the initial Gaussian distributions for the state, ballistic coefficients, and reduced-order density; propagated them for two days; and compared the final position with the position uncertainty according to the propagated covariance matrix. Figure 4 shows the 1-, 2-, and 3- $\sigma$ ellipsoids computed using the propagated position covariance matrix and 1000 Monte Carlo samples. The  $3-\sigma$  ellipsoid in this figure corresponds to the  $P_1$  ellipsoid in Figs. 5b and 5c. The Gaussian PDF provided by the covariance matrix seems to be a good approximation of the true PDF. This is confirmed by Table 4, which shows the fraction of Monte Carlo samples within the  $\sigma$  bounds and the expected fraction for a three-dimensional Gaussian distribution. The expected and true fractions differ by a maximum of 1.3%, and so the Gaussian assumption for the position PDF is valid. In future work, other multivariate normality tests will be employed to assess the Gaussianity of the PDFs [25].

#### C. Probability of Collision Including Density Uncertainty

Using the propagated covariance for the position, we computed  $P_c$  with density uncertainty. Figure 5 shows the  $3-\sigma$  ellipsoids depicting the position covariance for objects 1 and 2 and the combined covariance at the TCA for test case S0. Figure 5a shows the covariance without considering density uncertainty, whereas Figs. 5b and 5c include density uncertainty. In addition, the combined covariance in Fig. 5c accounts for cross correlation, whereas the combined covariance in Fig. 5b does not. As expected, the covariance gets inflated when uncertainties due to density are included (note the different scales of the axes in Figs. 5a–5c). Furthermore, Fig. 5c shows that accounting for the cross correlation can have a large effect on the combined covariance (i.e., the covariance of the miss distance) by making it less diffuse.

Table 5 shows the  $P_c$  computed for the different conjunction scenarios, with and without considering uncertainties in density. Let us first consider the fourth and fifth columns, which show  $P_c$  in the case of ignoring and including the density uncertainty without considering cross correlation. We can see that, due to the larger covariance when including density uncertainties,  $P_c$  including density errors  $P_c^{\rho}$  is smaller than  $P_c$  without density errors  $P_c^{w/\rho}$  for very close approaches (see cases S0 and D0) and  $P_c^{\rho}$  is larger than  $P_c^{w/\rho}$  for more distant approaches (see cases S1, S2, D1, and D2). This effect of density uncertainty on  $P_c$  is as expected; see, e.g., Ref. [11].

# D. Effect of Cross Correlation

The position covariances of the two objects are correlated because they fly through the same atmosphere. Therefore, we computed the  $P_c$  that accounts for the effect of cross correlation  $P_c^{\rho, \text{corr}}$ , as described in Sec. II.F. The resulting  $P_c$  is shown in the sixth column in Table 5.  $P_c^{\rho, \text{corr}}$  is larger than  $P_c^{\rho}$  for very close approaches (see cases S0 and D0) and smaller than  $P_c^{\rho}$  for distant approaches. This is as expected because accounting for the cross correlation results in a smaller covariance.

To verify the calculation of the  $P_c$  considering cross correlation, we performed a Monte Carlo analysis to compute the expected  $P_c$  with atmospheric density uncertainty. Note that 10,000 random initial density states were sampled from the initial density PDF; and for each sample, the  $P_c$  considering only initial state errors was computed. The mean  $P_c$  value has converged after 10,000 Monte Carlo runs and shows minimal variations after 10,000 runs. Figure 6 shows the probability distribution of  $P_c$  for test case S0. The mean  $P_c$  was found to be  $2.35 \times 10^{-3}$ . For the same test case,  $P_c^{\rho, \text{corr}}$  computed by considering density uncertainty and cross correlation is  $1.72 \times 10^{-3}$ ; whereas  $P_c^{\rho}$  without considering cross correlation due to density uncertainty is  $9.33 \times 10^{-5}$ , and  $P_c^{\text{w}/\rho}$  without considering uncertainty in the density is  $4.03 \times 10^{-3}$ . Clearly, correcting for cross correlation improves the  $P_c$  estimate. In particular, for such a high  $P_c$  case, it is

<sup>††</sup>Data available online at http://tinyurl.com/densitysets [retrieved 10 May 2022].

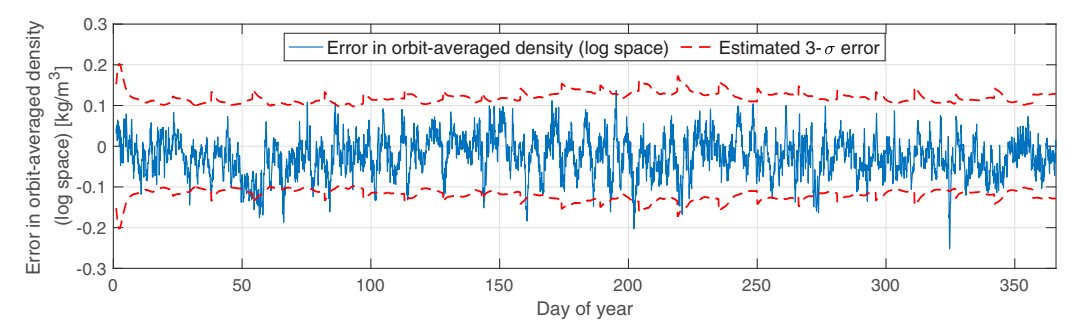


Fig. 1 Error in RODM-estimated orbit-averaged density and estimated 3-σ error in log space along CHAMP's orbit in 2007.

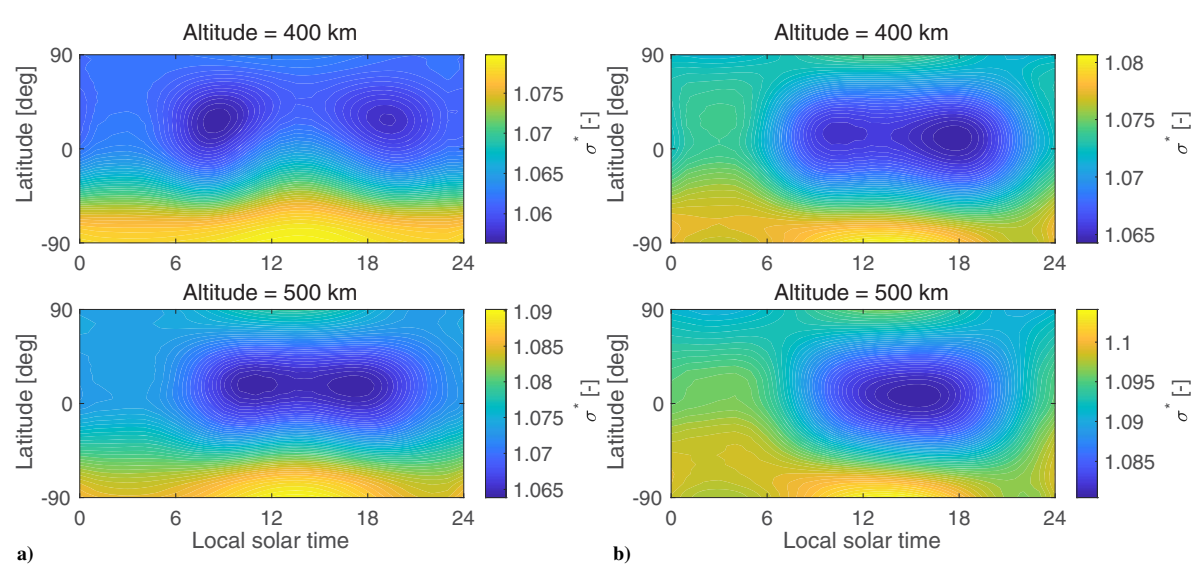


Fig. 2 Multiplicative standard deviation ( $\sigma^* = 10^{\sigma}$  where  $\sigma$  is the standard deviation in log space;  $\sigma^* = 1$  means  $\sigma = 0$ ) in predicted density at 400 and 500 km altitudes: a) uncertainty in estimated density after 10-day estimation 11 February 2003, and b) uncertainty in predicted density after two-day prediction 13 February 2003.

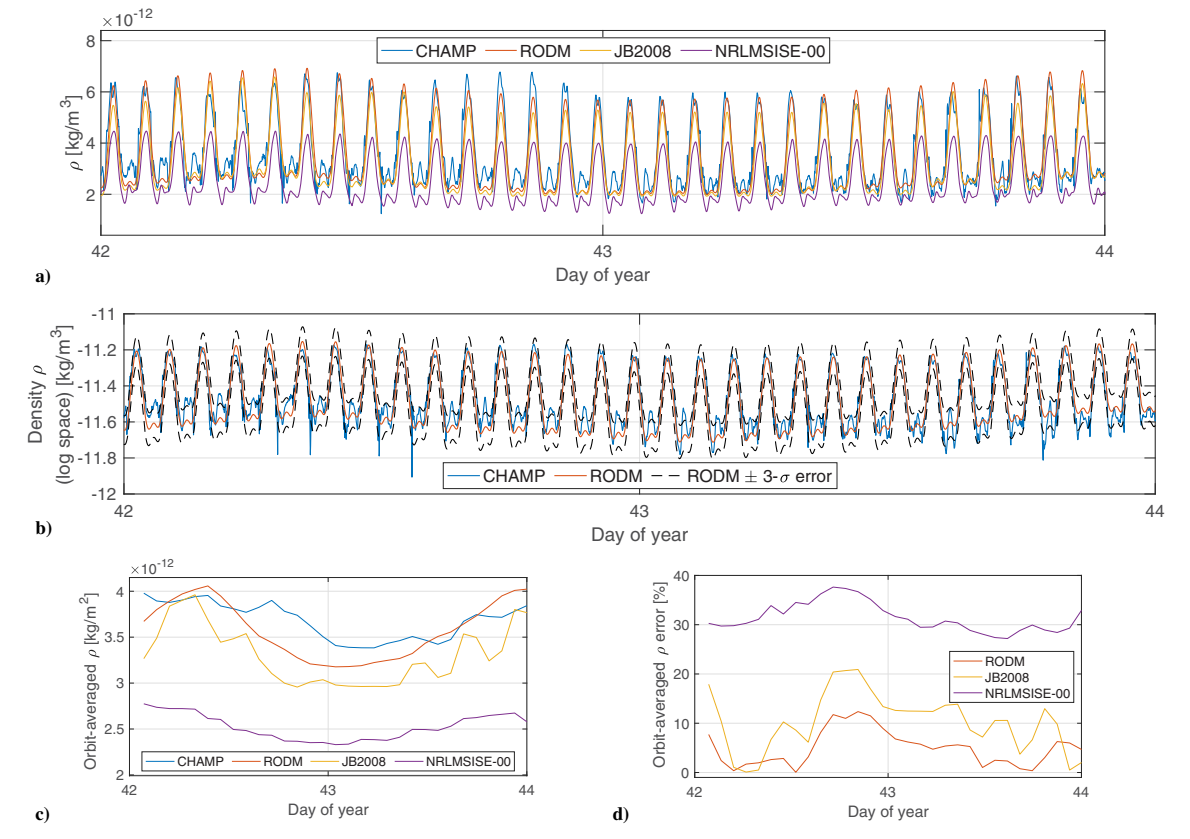


Fig. 3 Density along CHAMP orbit according to CHAMP accelerometer-derived data, RODM prediction, and JB2008 and NRLMSISE-00 models from 11 to 13 February 2003: a) predicted density, b)  $3-\sigma$  uncertainty in RODM-predicted density; c) orbit-averaged density; d) orbit-averaged density error.

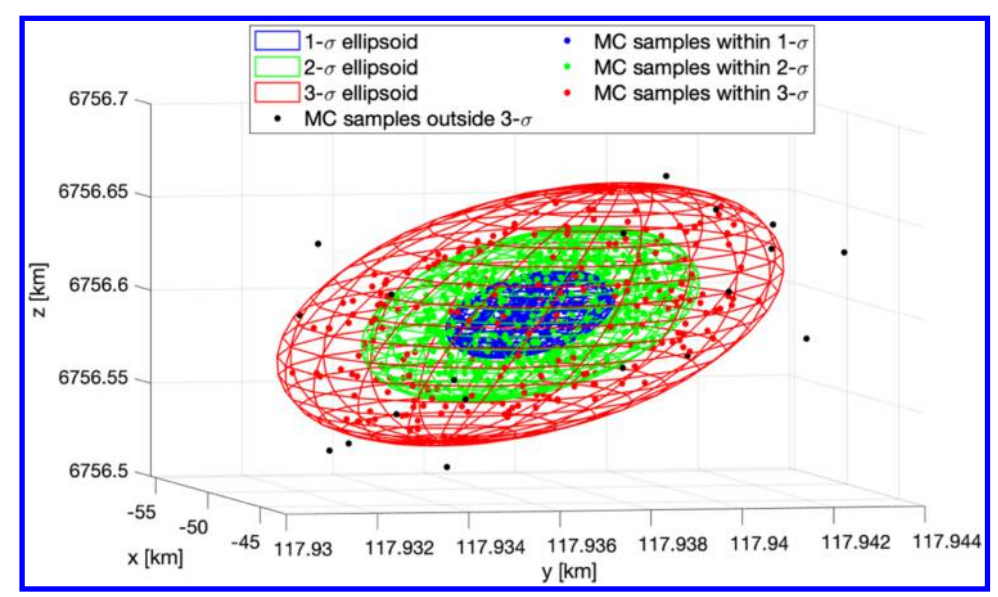


Fig. 4 Monte Carlo (MC) samples versus  $1-\sigma$ ,  $2-\sigma$ , and  $3-\sigma$  ellipsoids according to position covariance matrix.

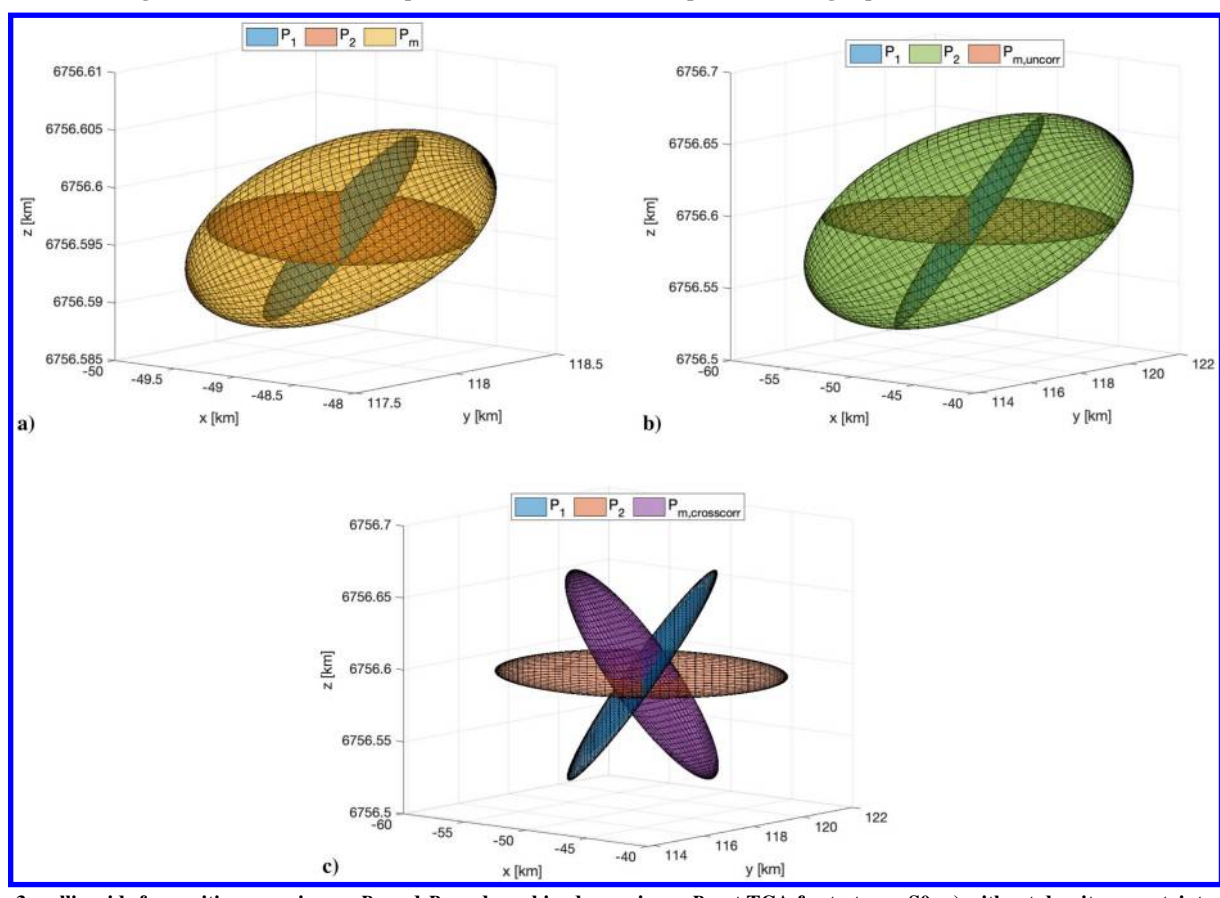


Fig. 5  $3-\sigma$  ellipsoids for position covariances  $P_1$  and  $P_2$  and combined covariance  $P_m$  at TCA for test case S0: a) without density uncertainty, b) with density uncertainty that is assumed to be uncorrelated, and c) with density uncertainty and considering cross correlation. Note that a larger scale was used for Fig. 5a as compared to Figs. 5b and 5c.

Table 4 Fraction of Monte Carlo samples inside 1- $\sigma$ , 2- $\sigma$ , and 3- $\sigma$  ranges according to unscented covariance propagation<sup>a</sup>

Range	Expected fraction of samples inside range	Fraction of MC samples inside range
1-σ	0.1987	0.200
$2-\sigma$	0.7385	0.748
3-σ	0.9707	0.979

<sup>&</sup>lt;sup>a</sup>MC using 1000 samples that were sampled from normal distributions in MEE,  $\beta$ , and reduced-order states.

important to take cross correlation into account because  $P_c$  without considering cross correlation is severely underestimating the realistic  $P_c$ . On the other hand, for the larger miss distances (cases S2 and D2), accounting for cross correlation results in a lower  $P_c$  because of a smaller combined covariance. These findings are in agreement with Casali et al. [13], who showed that accounting for cross correlation can both increase or decrease the  $P_c$ , depending on the geometry.

For the conjunction scenarios where the two objects have different  $\beta$ , the effect of cross correlation on  $P_c$  is much smaller. This is because the effect of drag on object 2 is smaller due to a smaller  $\beta$ . The smaller  $\beta$  reduces the effect of density errors on  $P_c$ , and thus

			Probability of collision $P_c$				
			No donoity	With density uncertainty			
Scenario	Test case	DCA, km	No density uncertainty $P_c^{w/o}$	No correlation $P_c^{\rho}$	Cross correlation $P_c^{\rho, \text{corr}}$	MC: mean $P_c^{\rho, \text{MC}}$	
Same β	S0	0.00031	$4.03 \times 10^{-3}$	$9.33 \times 10^{-5}$	$1.72 \times 10^{-3}$	$2.35 \times 10^{-3}$	
	S1	0.92375	$1.03 \times 10^{-7}$	$7.12 \times 10^{-5}$	$2.68 \times 10^{-5}$	$9.58 \times 10^{-7}$	
	S2	1.84755	$2.32\times10^{-22}$	$3.16\times10^{-5}$	$6.60 \times 10^{-11}$	$4.13 \times 10^{-17}$	
Different $\beta$	D0	0.00015	$5.33 \times 10^{-3}$	$1.67 \times 10^{-4}$	$2.00 \times 10^{-4}$	$2.05 \times 10^{-4}$	
	D1	0.92412	$2.04 \times 10^{-9}$	$1.02 \times 10^{-4}$	$1.11 \times 10^{-4}$	$1.11 \times 10^{-4}$	
	D2	1.84792	0.0	$2.35 \times 10^{-5}$	$1.89 \times 10^{-5}$	$1.97 \times 10^{-5}$	

Table 5 Probability of collision  $P_c$  for two  $\beta$  scenarios and for different distances of close approach computed with and without considering density uncertainties and cross correlation, as well as by using Monte Carlo analysis

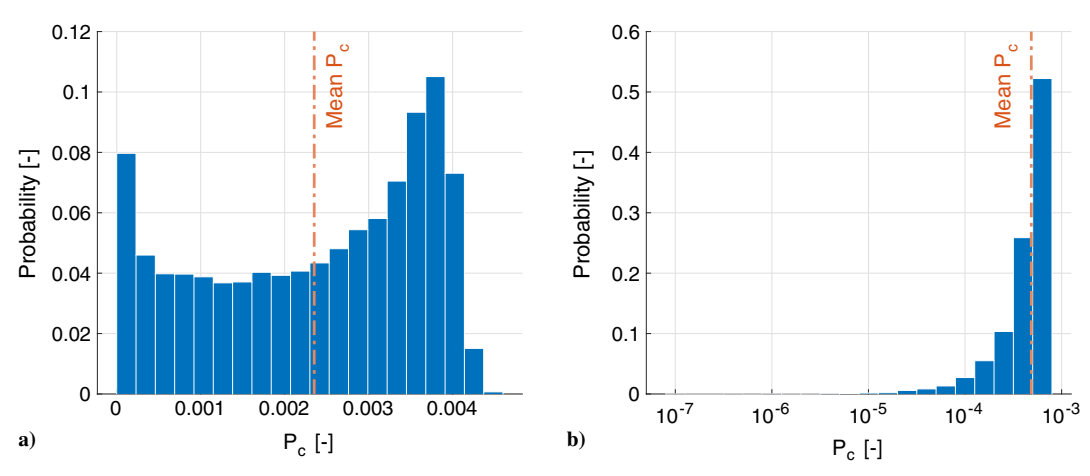


Fig. 6 Probability distribution function of  $P_c$  as a result of uncertainties in the atmospheric density for test case S0: a) linear scale, and b) log scale.

results in a smaller cross correlation. Still, for the high  $P_c$  (case D0), the cross-correlation correction improves the collision probability estimate;  $P_c^{\rho, \text{corr}}$  is closer to the estimated true  $P_c$  (given by  $P_c^{\rho, \text{MC}}$ ) than  $P_c^{\rho}$ . In all cases, accounting for cross correlation results in a better estimate of  $P_c$  (i.e., closer to  $P_c^{\rho, \text{MC}}$ ). These results show the following:

- 1) One should compensate for the cross correlation due to density errors.
- 2) Our approach to account for the effect of cross correlation provides improved  $P_c$  estimates.

# V. Conclusions

This Note has demonstrated how atmospheric density uncertainties can be estimated and included for conjunction assessment. The recently developed dynamic reduced-order density model was used to estimate the density using TLE data, and the uncertainty in the estimates was quantified by using a Kalman filter. The benefit of this approach is 1) the uncertainty in the density can be quantified, 2) the uncertainty forward can be propagated, and 3) the uncertainty is location (i.e., latitude, longitude, and altitude) and time (i.e., solar activity) dependent. The estimated uncertainties in the density were considered for collision probability calculation by propagating the state and density uncertainties simultaneously to obtain the position covariance at the TCA. In addition, because the position covariances of two objects flying through the same atmosphere are correlated, the effect of cross correlation due to density errors on the  $P_{\it c}$  was accounted for.

The density uncertainty was shown to have a significant effect on  $P_c$  for well-tracked space objects where the contributions of density uncertainty to position uncertainty are dominant. Including density uncertainty increases the position covariances and results in lower  $P_c$  for very close approaches and higher  $P_c$  for more distant approaches as compared to ignoring errors due to density. Moreover, the results showed that it is important to consider the effect of cross correlation

on  $P_c$ , especially when the effect of density errors on the orbit is similar for both objects. In particular, for very close approaches, ignoring the cross correlation can result in severe underestimation of the collision probability. The presented approach provides the distinctive capability to quantify the uncertainty in atmospheric density and to include this uncertainty for conjunction assessment while taking into account the dependence of the density model errors on location and time.

## Acknowledgments

The authors wish to acknowledge the support of this work by the U.S. Air Force Office of Scientific Research under contract number FA9550-18-1-0149, issued by Erik Blasch, and the National Science Foundation under award number NSF-PHY-2028125.

# References

- [1] Continuing Kepler's Quest: Assessing Air Force Space Command's Astrodynamics Standards, The National Academies Press, Washington, D.C., 2012, pp. 19–43, https://www.nap.edu/catalog/13456/continuing-keplers-quest-assessing-air-force-space-commands-astrodynamics-standards [retrieved 10 May 2022]. https://doi.org/10.17226/13456
- [2] Vallado, D. A., and Finkleman, D., "A Critical Assessment of Satellite Drag and Atmospheric Density Modeling," *Acta Astronautica*, Vol. 95, Feb.–March 2014, pp. 141–165. https://doi.org/10.2514/6.2008-6442
- [3] He, C., Yang, Y., Carter, B., Kerr, E., Wu, S., Deleflie, F., Cai, H., Zhang, K., Sagnières, L., and Norman, R., "Review and Comparison of Empirical Thermospheric Mass Density Models," *Progress in Aero-space Sciences*, Vol. 103, Nov. 2018, pp. 31–51. https://doi.org/10.1016/j.paerosci.2018.10.003
- [4] Anderson, R. L., Born, G. H., and Forbes, J. M., "Sensitivity of Orbit Predictions to Density Variability," *Journal of Spacecraft and Rockets*, Vol. 46, No. 6, 2009, pp. 1214–1230. https://doi.org/10.2514/6.2008-6443

- [5] Emmert, J., Warren, H., Segerman, A., Byers, J., and Picone, J., "Propagation of Atmospheric Density Errors to Satellite Orbits," *Advances in Space Research*, Vol. 59, No. 1, 2017, pp. 147–165. https://doi.org/10.1016/j.asr.2016.07.036
- [6] Schiemenz, F., Utzmann, J., and Kayal, H., "Propagation of Grid-Scale Density Model Uncertainty to Orbital Uncertainties," *Advances in Space Research*, Vol. 65, No. 1, 2019, pp. 407–418. https://doi.org/10.1016/j.asr.2019.10.013
- [7] Cefola, P. J., Proulx, R. J., Nazarenko, A. I., and Yurasov, V. S., "Atmospheric Density Correction Using Two Line Element Sets as the Observation Data," *Advances in the Astronautical Sciences, Astro*dynamics 2003, Vol. 116, Aug. 2004, pp. 1239–1252.
- [8] Storz, M. F., Bowman, B. R., Branson, M. J. I., Casali, S. J., and Tobiska, W. K., "High Accuracy Satellite Drag Model (HASDM)," Advances in Space Research, Vol. 36, No. 12, 2005, pp. 2497–2505. https://doi.org/10.1016/j.asr.2004.02.020
- [9] Doornbos, E., Klinkrad, H., and Visser, P., "Use of Two-Line Element Data for Thermosphere Neutral Density Model Calibration," *Advances in Space Research*, Vol. 41, No. 7, 2008, pp. 1115–1122. https://doi.org/10.1016/j.asr.2006.12.025
- [10] Bussy-Virat, C. D., Ridley, A. J., and Getchius, J. W., "Effects of Uncertainties in the Atmospheric Density on the Probability of Collision Between Space Objects," *Space Weather*, Vol. 16, No. 5, 2018, pp. 519–537. https://doi.org/10.1029/2017sw001705
- [11] Hejduk, M. D., and Snow, D. E., "The Effect of Neutral Density Estimation Errors on Satellite Conjunction Serious Event Rates," *Space Weather*, Vol. 16, No. 7, 2018, pp. 849–869. https://doi.org/10.1029/2017SW001720
- [12] Coppola, V. T., Woodburn, J., and Hujsak, R., "Effects of Cross Correlated Covariance on Space-Craft Collision Probability," *Advances in the Astronautical Sciences, Spaceflight Mechanics* 2004, Vol. 119, 2005, pp. 1239–1252.
- [13] Casali, S., Hall, D., Snow, D., Hejduk, M., Johnson, L., Skrehart, B., and Baars, L., "Effect of Cross-Correlation of Orbital Error on Probability of Collision Determination," *Advances in the Astronautical Sciences, Astrodynamics* 2018, Vol. 167, 2019, pp. 2083–2096.
- [14] Mehta, P. M., Linares, R., and Sutton, E. K., "A Quasi-Physical Dynamic Reduced Order Model for Thermospheric Mass Density via Hermitian Space-Dynamic Mode Decomposition," *Space Weather*, Vol. 16, No. 5, 2018, pp. 569–588. https://doi.org/10.1029/2018SW001840
- [15] Yurasov, V. S., Nazarenko, A. I., Alfriend, K. T., and Cefola, P. J., "Reentry Time Prediction Using Atmospheric Density Corrections," *Journal of Guidance, Control, and Dynamics*, Vol. 31, No. 2, 2008, pp. 282–289. https://doi.org/10.2514/1.26593

- [16] Shoemaker, M. A., Wohlberg, B., and Koller, J., "Atmospheric Density Reconstruction Using Satellite Orbit Tomography," *Journal of Guidance, Control, and Dynamics*, Vol. 38, No. 4, 2015, pp. 685–698. https://doi.org/10.2514/1.G000088
- [17] Mehta, P. M., and Linares, R., "A New Transformative Framework for Data Assimilation and Calibration of Physical Ionosphere-Thermosphere Models," *Space Weather*, Vol. 16, No. 8, 2018, pp. 1086–1100. https://doi.org/10.1029/2018SW001875
- [18] Gondelach, D. J., and Linares, R., "Real-Time Thermospheric Density Estimation via Two-Line Element Data Assimilation," *Space Weather*, Vol. 18, No. 2, 2020, Paper e2019SW002356. https://doi.org/10.1029/2019SW002356
- [19] Mehta, P. M., and Linares, R., "Real-Time Thermospheric Density Estimation from Satellite Position Measurements," *Journal of Guidance, Control, and Dynamics*, Vol. 43, No. 9, 2020, pp. 1656–1670.
- https://doi.org/10.2514/1.G004793
  [20] Gondelach, D. J., and Linares, R., "Real-Time Thermospheric Density Estimation via Radar and GPS Tracking Data Assimilation," *Space Weather*, Vol. 19, No. 4, 2021, Paper e2020SW002620. https://doi.org/10.1029/2020SW002620
- [21] Wan, E. A., and Van Der Merwe, R., "The Unscented Kalman Filter," Kalman Filtering and Neural Networks, Wiley, New York, 2001, pp. 221–280, Chap. 7. https://doi.org/10.1002/0471221546.ch7
- [22] Alfano, S., "A Numerical Implementation of Spherical Object Collision Probability," *Journal of Astronautical Sciences*, Vol. 53, No. 1, 2005, pp. 103–109. https://doi.org/10.1007/bf03546397
- [23] Hemenway, B., Welser, W., and Baiocchi, D., "Achieving Higher-Fidelity Conjunction Analyses Using Cryptography to Improve Information Sharing," RAND Corp. TR RR-344-AF, Santa Monica, CA, 2014.
- [24] Julier, S. J., and Uhlmann, J. K., "New Extension of the Kalman Filter to Nonlinear Systems," *Signal Processing, Sensor Fusion, and Target Recognition VI*, Vol. 3068, International Soc. for Optics and Photonics, Bellingham, WA, 1997, pp. 182–193. https://doi.org/10.1117/12.280797
- [25] Mardia, K., "Tests of Univariate and Multivariate Normality," Handbook of Statistics: Analysis of Variance, Vol. 1, Elsevier, New York, 1980, pp. 279–320. https://doi.org/10.1016/S0169-7161(80)01011-5
- [26] Sutton, E. K., "Effects of Solar Disturbances on the Thermosphere Densities and Winds from CHAMP and GRACE Satellite Accelerometer Data," Ph.D. Thesis, Univ. of Colorado at Boulder, Boulder, CO, Oct. 2008.